Contribution from the ARC Unit of Nitrogen Fixation and the School of Molecular Sciences, University of Sussex, Brighton BN1 9QJ, U.K., and Chemistry Department, State University of New York at Albany, Albany, New York 12222

Electrochemical Generation of Sulfur-Ligated Molybdenum(II) and Molybdenum(III) Substrate Binding Sites. Preparation and Crystal Structures of $[MoCl(S_2CNEt_2)_2(Ph_2PCH_2CH_2PPh_2)][BF_4]$ and $[MoCl(S_2CNEt_2)_2(PPh_2Me)_2][PF_6]$ and the Mechanism of Their Electrochemical Reduction

JONATHAN R. DILWORTH,*† BRYAN D. NEAVES,† CHRISTOPHER J. PICKETT,*† JOSEPH CHATT,‡ and JON A. ZUBIETA*§

Received March 10, 1983

The complexes $[MoX(S_2CNR_2)_2P_2][Y]$ or $[MoX_2(S_2CNR_2)_2P]$ (R_2 = Me_2, Et_2, or $(CH_2)_5$; X = Cl or Br; Y = Cl, PF_6, BF_4, or BPh_4; P = $^1/_2$ $Ph_2PCH_2CH_2PPh_2$, PPh_2Me, PMe_2Ph, or PEt_2Ph) are prepared from $[MoOX_2(S_2CNR_2)_2]$ and P. The crystal and molecular structures of $[MoCl(S_2CNEt_2)_2(dppe)][BF_4]$ (I) and $[MoCl(S_2CNEt_2)_2(PPh_2Me)_2][PF_6]$ (VII) have been determined by single-crystal X-ray diffraction methods. Crystal data for complex I: space group $P\bar{1}$, a = 11.422 (7) Å, b = 11.902 (9) Å, c = 16.900 (8) Å, α = 104.64 (1)°, β = 101.65 (2)°, γ = 103.34 (1)°, V = 2078.60 Å^3, Z = 2, R = 6.8% from 5429 reflections. Crystal data for complex VII: space group $P2'2'2'$, a = 9.132 (7) Å, b = 17.028 (7) Å, c = 28.084 (7) Å, V = 4367.42 Å^3, Z = 4, R = 9.8% from 2783 reflections. Both complexes have distorted pentagonal-bipyramidal geometries. Chemical or electrochemical reduction of $[MoCl(S_2CNR_2)_2(dppe)]^+$ under CO gives $[Mo(CO)(S_2CNR_2)_2(dppe)]$, whereas under N_2 or Ar dimeric $[\{Mo(S_2CNR_2)_2(dppe)\}_2]^{2+}$ is formed. The redox chemistry of these species and other intermediates has been studied by a range of electrochemical techniques, and reduction mechanisms are proposed, together with the implications for the binding of small molecules to the reductively generated site.

Introduction

Recent EXAFS studies of the enzyme nitrogenase have shown that the molybdenum is ligated predominantly by sulfur.[1] However, there is to date only one very unstable complex $[Mo(N_2)_2(PhSCH_2CH_2SPh)(PMe_2Ph)_2]$[2] that contains both sulfur and dinitrogen. Moreover, there are very few examples of the binding of any of the alternative nitrogenase substrates such as CH≡CH or MeNC to a sulfur-ligated molybdenum.[3,4] However, we report our attempts to generate Mo(II) and Mo(III) binding sites with four S and two P donors by the electrochemical and chemical reduction of some Mo(IV) chloro–dithiocarbamato–phosphine complexes and to study their interaction with various substrates. The Mo(IV) precursors of the type $[MoX(S_2CNR_2)_2P_2][Y]$ or $[MoX_2(S_2CNR_2)_2P]$ (R = Me, Et, or $(CH_2)_5$; X = Cl or Br; Y = Cl, PF_6, BF_4, or BPh_4, P = $^1/_2$ $Ph_2PCH_2CH_2PPh_2$ (dppe), PPh_2Me, PEt_2Ph, or PMe_2Ph) were prepared by reaction of $[MoOX_2(S_2CNR_2)_2]$ with the appropriate phosphine, the product depending on both solvent and phosphine.

Results and Discussion

Preparation of Dithiocarbamato Complexes of Molybdenum(IV). Neutral Species. Reaction of the complexes $[MoOX_2(S_2CNR_2)_2]$ (X = Cl or Br; R_2 = Et_2, Me_2, or piperidyl) with 2 equiv of PMe_2Ph in refluxing THF gives the green complexes $[MoX_2(S_2CNR_2)_2PMe_2Ph]$ in 64–70% yield. The complexes prepared by this method are listed in Table I (supplementary material). They are air stable in the solid state and in solution, and conductivity measurements show that they are nonelectrolytes in methyl cyanide and nitrobenzene solutions. The far-IR spectrum of $[MoCl_2(S_2CNEt_2)_2PMe_2Ph]$ has strong bands at 295, 357, and 374 cm^{-1} assignable to ν(Mo–Cl) and ν(Mo–S). The ^{1}H NMR spectrum, in $CDCl_3$, of the complexes show they are paramagnetic. The complexes are EPR inactive, consistent with their being d^2 Mo(IV) species. Complex XII has a magnetic susceptibility of 2.57 μ_B at 25 °C, a typical value for a high-spin Mo(IV) complex.[5,6]

Cationic Complexes. The complexes $[MoOX_2(S_2CNR_2)_2]$ (X = Cl or Br; R_2 = Me_2 or Et_2) are reduced by mono- and di(tertiary phosphines) in methanol at room temperature to give the complexes $[MoX(S_2CNR_2)_2(P_2)]X$ (P_2 = $(PMe_2Ph)_2$, $(PPh_2Me)_2$, $(PEt_2Ph)_2$, or $Ph_2PCH_2CH_2PPh_2$) in 65–70% yield. The complexes are summarized in Table I. All are air stable and have conductivities in methyl cyanide typical for 1:1 electrolytes. The ^{1}H NMR spectra of the complexes show they are paramagnetic, but they are also EPR silent. Magnetic susceptibility measurements on selected complexes are consistent with Mo(IV) species in a high-spin state.[5,6] The IR spectrum of $[MoCl(S_2CNEt_2)_2(dppe)][BF_4]$ has bands at 290, 299, and 369 cm^{-1} attributable to ν(Mo–S). A somewhat surprising feature of these complexes is the difference in color between the olive green diphosphine complexes and the orange monophosphine complexes. This is reflected in the UV–visible spectra of complexes I and VII, summarized in Table II. The diphosphine complex has characteristic absorptions at 27 000, 25 800, 24 900, and 22 800 cm^{-1}. The absorptions of the monophosphine complex are shifted to 27 300, 24 400, 22 000, and 19 500 cm^{-1}. The spectroscopic properties outlined above

Table II. UV-Visible Absorptions of $[MoCl(S_2CNEt_2)_2(dppe)][BF_4]$ and $[MoCl(S_2CNEt_2)_2(PPh_2Me)_2][PF_6]$

complex	λ_{max}, cm^{-1} [a]	$10^{-3}\epsilon$, mol^{-1} L cm^{-1}
$[MoCl(S_2CNEt_2)_2(dppe)][BF_4]$	27 800	4.3
	25 800	6.4
	24 900	7.7
	22 800	4.0
$[MoCl(S_2CNEt_2)_2(PPh_2Me)_2][PF_6]$	27 300	7.4
	24 400	3.1
	22 000	3.0
	19 500	3.4

[a] Spectra were recorded in acetonitrile solution.

† ARC Unit of Nitrogen Fixation, University of Sussex.
‡ School of Molecular Sciences, University of Sussex.
§ State University of New York at Albany.

(1) Cramer, S. P.; Hodgson, K. O.; Stiefel, E. I.; Newton, W. E. *J. Am. Chem. Soc.* **1978**, *100*, 2748.
(2) Aresta, M.; Sacco, A. *Gazz. Chim. Ital.* **1972**, *102*, 755.
(3) Schneider, P. W.; Bravard, D. C.; McDonald, J. W.; Newton, W. E. *J. Am. Chem. Soc.* **1972**, *94*, 8640. Newton, W. E.; McDonald, J. W.; Corbin, J. L.; Richard, L.; Weiss, R. *Inorg. Chem.* **1980**, *19*, 1997. Templeton, J. L.; Ward, B. C.; Chen, G. J. J.; McDonald, J. W.; Newton, W. E. *Ibid.* **1981**, *20*, 1248.
(4) Maata, E. A.; Wentworth, R. A. D. *Inorg. Chem.* **1979**, *18*, 524.
(5) Allen, E. A.; Freeman, K.; Fowles, G. W. A. *J. Chem. Soc.* **1965**, 1646.
(6) Butcher, A. V.; Chatt, J. *J. Chem. Soc. A* **1970**, 2652.

0020-1669/83/1322-3524$01.50/0

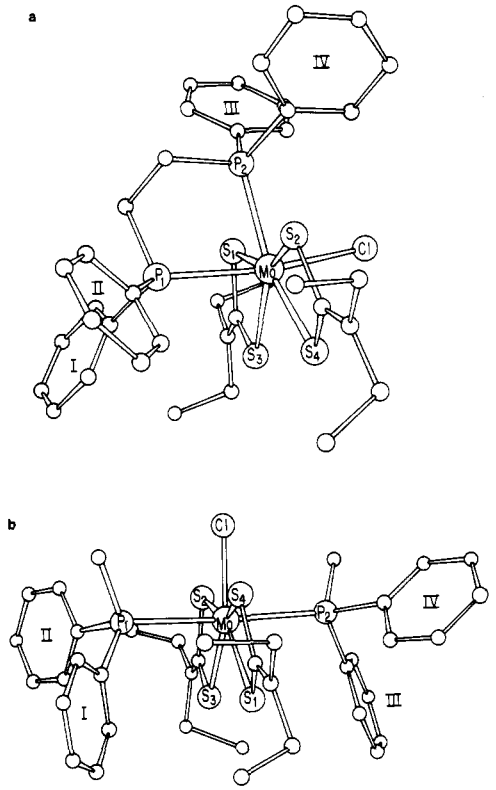

Figure 1. (a) Perspective view of $[MoCl(S_2CNEt_2)_2(dppe)][BF_4]$; atom labeling for N and C omitted for clarity. (b) Perspective view of $[MoCl(S_2CNEt_2)_2(PPh_2Me)_2][PF_6]$; atom labels for N and C omitted for clarity.

Table III. Experimental Summary of Crystal Data

	$[MoCl(S_2CNEt_2)_2$-(dppe)][BF_4]	$[MoCl(S_2CNEt_2)_2$-$(PPh_2Me)_2][PF_6]$
fw	913.20	973.38
a, Å	11.422 (7)	9.132 (7)
b, Å	11.902 (9)	17.028 (8)
c, Å	16.900 (8)	28.084 (7)
α, deg	104.64 (1)	90.00
β, deg	101.65 (2)	90.00
γ, deg	103.34 (1)	90.00
V, Å^3	2078.60	4367.42
cryst form	triclinic	orthorhombic
syst absences	none	$h00$, $h = 2n + 1$; $0k0$, $k = 2n + 1$; $00l$, $l = 2n + 1$
space group	$P\bar{1}$	$P2_12_12_1$
Z	2	4
ρ(calcd), g cm^{-3}	1.46	1.48
ρ(found), g cm^{-3}	1.43 (2)	1.50 (2)
F(000)	935.98	1991.82
λ(Cu), Å	K$\bar{\alpha}$, 1.5418	K$\bar{\alpha}$, 1.5418
μ(Cu Kα), cm^{-1}	6.29	41.57
reflcns	5429 symmetry-independent reflcns for $2 < 2\theta < 65°$ with $I_o > 2.5\sigma(I_o)$ (7231 collcd)	2783 symmetry-independent reflcns for $2 < 2\theta < 6°$ with $I_o > 2.5\sigma(I_o)$ (3798 collcd)

are not sufficient to differentiate between the possible structures for the complexes, and accordingly the structures of complexes I and VII have been determined by X-ray diffraction.

Crystal Structure. These showed that both complexes display distorted pentagonal-bipyramidal geometry. Perspective views of the molecular geometry giving the atom-labeling schemes are presented in Figure 1. Cell parameters and experimental conditions for data collection and reduction and structure solutions are summarized in Table III. Final atomic positional and thermal parameters are given in Tables IVa and IVb (supplementary material) for $[MoCl(S_2CNEt_2)_2(dppe)][BF_4]$ and $[MoCl(S_2CNEt_2)_2(PPh_2Me)_2][PF_6]$, respectively. Relevent bond lengths and angles are given in Table V (expanded listings are given in the supplementary material). Nonbonding interactions defining the polyhedral edges are listed in Table VIa and VIb (supplementary material). Only small deviations from idealized geometry are observed in both complexes; however, it is evident from the P(1)–Mo–Cl angle [176.5 (3)°] in VII that the chelating diphopshine ligand applies steric constraints to the structure of I. Clearly, a diphosphine ligand spanning

Table V. Selected Molecular Bond Distances (Å) and Angles (deg)

a. $[MoCl(S_2CNEt_2)_2(dppe)][BF_4]$

Bond Distances

Mo-P(1)	2.564 (2)	C(2)-N(2)	1.30 (1)
Mo-P(2)	2.604 (2)	N(1)-C(7)	1.48 (1)
Mo-Cl	2.404 (2)	N(1)-C(8)	1.49 (1)
Mo-S(1)	2.492 (2)	N(2)-C(3)	1.48 (1)
Mo-S(2)	2.501 (2)	N(2)-C(4)	1.49 (1)
Mo-S(3)	2.483 (2)	C(7)-C(9)	1.50 (2)
Mo-S(4)	2.482 (2)	C(8)-C(10)	1.49 (1)
S(1)-C(1)	1.72 (1)	C(3)-C(5)	1.51 (2)
S(3)-C(1)	1.70 (1)	C(4)-C(6)	1.50 (2)
S(2)-C(2)	1.71 (1)	C(15)-C(16)	1.53 (1)
S(4)-C(2)	1.71 (1)	av C-C, ring I	1.38 (1)
P(1)-C(11)	1.83 (1)	av C-C, ring II	1.39 (1)
P(1)-C(12)	1.84 (1)	av C-C, ring III	1.38 (2)
P(1)-C(15)	1.83 (1)	av C-C, ring IV	1.38 (1)
P(2)-C(13)	1.83 (1)	B-F(1)	1.35 (2)
P(2)-C(13)	1.83 (1)	B-F(2)	1.35 (2)
P(2)-C(16)	1.82 (1)	B-F(3)	1.24 (2)
C(1)-N(1)	1.31 (1)	B-F(4)	1.43 (2)

Bond Angles[a]

P(1)-Mo-P(2)	79.7 (1)	P(1)-Mo-Cl	170.0 (1)

b. $[MoCl(S_2CNEt_2)_2(PPh_2Me)_2][PF_6]$

Bond Distances

Mo-P(1)	2.584 (9)	C(1)-N(1)	1.30 (4)
Mo-P(2)	2.608 (9)	C(2)-N(2)	1.24 (4)
Mo-S(1)	2.496 (8)	N(1)-C(3)	1.51 (5)
Mo-S(2)	2.478 (9)	N(1)-C(4)	1.53 (5)
Mo-S(3)	2.479 (8)	N(2)-C(7)	1.57 (5)
Mo-S(4)	2.477 (9)	N(2)-C(8)	1.45 (5)
Mo-Cl	2.431 (9)	C(3)-C(5)	1.66 (6)
S(1)-C(1)	1.72 (3)	C(4)-C(6)	1.52 (6)
S(4)-C(1)	1.80 (4)	C(7)-C(9)	1.58 (7)
S(2)-C(2)	1.73 (3)	C(8)-C(10)	1.46 (7)
S(3)-C(2)	1.70 (3)	av C-C, rings	1.39 (5)
P(1)-C(11)	1.86 (2)	P(3)-F(1)	1.61 (4)
P(1)-C(12)	1.86 (3)	P(3)-F(2)	1.58 (4)
P(1)-C(15)	1.85 (4)	P(3)-F(3)	1.55 (9)
P(2)-C(13)	1.87 (3)	P(3)-F(4)	1.52 (8)
P(2)-C(14)	1.87 (3)	P(3)-F(5)	1.56 (7)
P(3)-C(16)	1.86 (4)	P(3)-F(6)	1.55 (6)

Bond Angles[a]

P(11)-Mo-P(2)	176.5 (3)	P(1)-Mo-Cl	90.1 (13)

[a] A complete list of bond angles is given in the supplementary material.

Table VIII. Electrochemical Data[a]

complex	$^1E^{RED}$, V vs. SCE	$\lvert E_p^{RED} - E_p^{OX} \rvert$, mV
$[MoCl(S_2CNEt_2)_2(dppe)][BF_4]$[b]	−0.28	80
$[MoCl(S_2CNMe_2)_2(dppe)][BF_4]$	−0.29	75
$[MoCl(S_2CNEt_2)_2(PPh_2Me)_2][PF_6]$	−0.48	90
$[MoCl(S_2CNEt_2)_2(PMe_2Ph)_2][BPh_4]$	−0.52	80
$[MoCl(S_2CNEt_2)_2(PEt_2Ph)_2][BPh_4]$	−0.56	50
range	±0.01	±5

[a] In 0.2 mol dm^{-3}; $[NBu_4][BF_4]$–CH_3CN at a Pt electrode. [b] Secondary redox processes observed with $E_p^{RED} = -0.57$ (2), −0.74 (3), −0.82 (4), and −1.28 (5) where numbers in parentheses refer to Figure 3.

axial and equatorial positions is preferred; distortions would be much greater if a dithiocarbamate ligand spanned these positions, evident from the normalized bite[7] of 1.14 for dithiocarbamate and 1.28 for dppe. These can be compared to the calculated value for an ideal pentagonal bipyramid (1.41). In both complexes I and VII S–Mo–S angles and Mo–S distances are typical for dithiocarbamato complexes.[8-13] The average Mo–P distance (2.590 Å) is comaprable to that found in $[MoCl_4(PMe_2Ph)_3]$ (2.577 Å),[14] longer than those found in most six-coordinate complexes, attributable to large nonbonding interactions associated with phosphine ligands in complexes of high coordination number. Reference to Table V shows that intraligand bond angles and distances are not unusual, and the C–N bond distances in the dithiocarbamate ligands are as expected from IR data.

The structures unequivocally show that in I the chelating diphosphine ligand is, as expected, in a cis configuration, whereas the monophosphine ligands in VII are in a trans configuration. Consequently, the most significant difference between I and VII is the position of the chloride ligand; in I it is in an axial position, with a shorter Mo–Cl bond than that observed in VII where the chlorine atom is in an equatorial position.

Chemical Reduction of the Cationic Complexes. Chemical reduction of complexes I and VII under argon and dinitrogen using sodium naphthalide or magnesium in THF yields intractable brown residues. However, reduction of $[MoCl(S_2CNR_2)_2(dppe)][Y]$ (I–V) with tin or zinc, under argon or dinitrogen, in dry methanol or methyl cyanide gives an orange product that can be precipitated from solution as a tetrafluoroborate, hexafluorophosphate, or tetraphenylborate salt. The tetrafluoroborate product is recrystallized as orange-red prisms. These new complexes no longer have an IR band attributable to ν(Mo–Cl), but a strong band in the region 1550–1490 cm^{-1} remains, assignable to ν(CN) of the dithiocarbamate ligands. The complexes are diamagnetic, and the ^1H NMR spectra are very complicated in the alkyl region. In the case of the dimethyldithiocarbamato complexes, eight resonances attributable to methyl groups are observed. Thus, each dithiocarbamate is in a unique environment with hindered rotation about the C–N bond. The ^1H NMR data indicate that at least a dimeric structure must be postulated. ^{31}P NMR spectra of the dimethyldithiocarbamato complexes show three 1:1 doublets, in the ratio 2:1:1. This is consistent with phosphine ligands also located in two distinct environments, with the phosphorus atoms of one ligand equivalent. The NMR data are presented in Table VII (supplementary material) together with other physical data for the complexes. Elemental analyses for complexes XVI–XIX are in accord with the formulation $[\{Mo(S_2CNR_2)_2(dppe)\}_2][Y]_2$ (R_2 = Me_2 or Et_2; Y = BF_4, PF_6, or BPh_4 when R_2 = Me_2 or Y = BPh_4 when R_2 = Et_2).

The NMR data indicate an asymmetric structure for the complexes, which possibly involves bridging dithiocarbamate and phosphine ligands; however, with no structural data it is not possible to assign a structure with any certainty. Electrochemical data are in accord with a structure that is at least dinuclear. The diamagnetism of the complexes suggests that the molybdenum atoms may be interacting. However, the asymmetry of the molecule indicates that a geometry similar to that observed for $[Mo_2(S_2COCH_3)_4]\cdot 2THF$ is unlikely.[8]

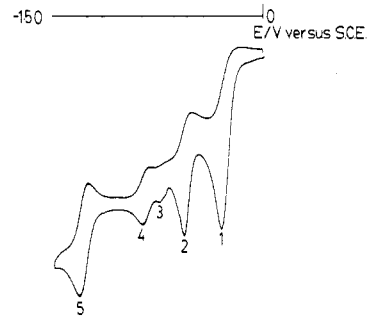

Figure 2. Cyclic voltammograms of $[MoCl(S_2CNEt_2)_2(dppe)][BF_4]$ (I) (0.01 V s^{-1}, Pt, 2.5 mmol dm^{-3}, 0.2 M $[n\text{-}Bu_4N][BF_4]$–CH_3CN).

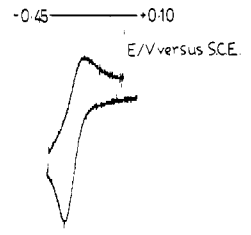

Figure 3. Cyclic voltammogram of $[MoCl(S_2CNEt_2)_2(dppe)][BF_4]$ (I) ((A) 30 V s^{-1}, (B) 100 V s^{-1}; Pt, 1.8 mmol dm^{-3}, 0.2 M $[n\text{-}Bu_4N][BF_4]$).

Attempts to prepare the monophosphine analogues of XVI–XIX have failed.

Reduction of complex I with tin under carbon monoxide in methanol gives a bright orange product, and simple manometry indicates that 1 mol equiv of CO is consumed during the reaction. Recyrstallization from dichloromethane–methanol gives bright orange prisms. The IR spectrum of the product shows a band at 1788 cm^{-1} assignable to ν(CO). Elemental analysis is in accord with the formulation $[Mo(CO)(S_2CNEt_2)_2(dppe)]$, the ^1H NMR shows a multiplet at 1.02 ppm and at 3.46 ppm assignable to the methyl and methylene protons of the dithiocarbamate ligands. The methylene protons of dppe are at 2.40 ppm. The preparation of this complex has recently been reported, using quite a different route,[15] involving reaction of $[Mo(CO)_2(S_2CNEt_2)_2]$ with dppe. This method has also been used to prepare the monophosphine analogues that cannot be prepared from complexes VII–XI by reduction under carbon monoxide. The behavior of the two series of complexes on electrochemical reduction is also different, and this is discussed in detail below.

Although the reductive generation of a π-acid binding site has clearly been demonstrated chemically, the mechanism of the reduction reaction was not clear. Accordingly, a detailed electrochemical study of the reduction of complexes I–XI was undertaken in the presence of a number of unsaturated small molecules such as N_2, CO, H_2, CH≡CH, and RNC.

Electrochemical Reduction of the Complexes $[MoCl(S_2CNR_2)_2(dppe)]^+$, $[MoCl]^+$ (R = Me or Et). Under Argon. The complexity of the electrode reactions of $[MoCl]^+$ is illustrated by the cyclic voltammogram of $[MoCl]^+$ (R = Et) at a Pt electrode in CH_3CN–0.2 M $[NBu_4][BF_4]$, which shows five discrete redox processes, labeled 1–5 in Figure 2. The behavior of the R = Me complex is very similar. The cyclic voltammetry of either complex in a THF electrolyte is *qualitatively* similar to that in CH_3CN.

Our attention has been mainly focused on the electrochemical behavior of the $[MoCl]^+$ (R = Et) complex, which

(7) Kepert, D. L. *Prog. Inorg. Chem.* **1979**, *25*, 40.
(8) Ricard, L.; Karaginannides, P.; Weiss, R. *Inorg. Chem.* **1973**, *12*, 2179.
(9) Ricard, L.; Estienne, J.; Weiss, R. *Inorg. Chem.* **1973**, *12*, 2183.
(10) Davis, R.; Hill, M. N. S.; Holloway, C. E.; Johnson, F. B. G.; Al-Obaidi, K. H. *J. Chem. Soc., Dalton Trans.* **1976**, 278.
(11) Dirand, J.; Ricard, L.; Weiss, R. *J. Chem. Soc., Dalton Trans.* **1976**, 278.
(12) Dirand, J.; Ricard, L., Weiss, R. *Transition Met. Chem. (Weinheim, Ger.)* **1975**, *1*, 2.
(13) Ricard, L.; Martin, C.; Wiess, R. *Inorg. Chem.* **1975**, *14*, 2300.
(14) Moss, J. R.; Shaw, B. L. *J. Chem. Soc. A* **1970**, 595.
(15) Crichton, B. A. L.; Dilworth, J. R.; Pickett, C. J.; Chatt, J. *J. Chem. Soc., Dalton Trans.* **1981**, 892.

Scheme I[a]

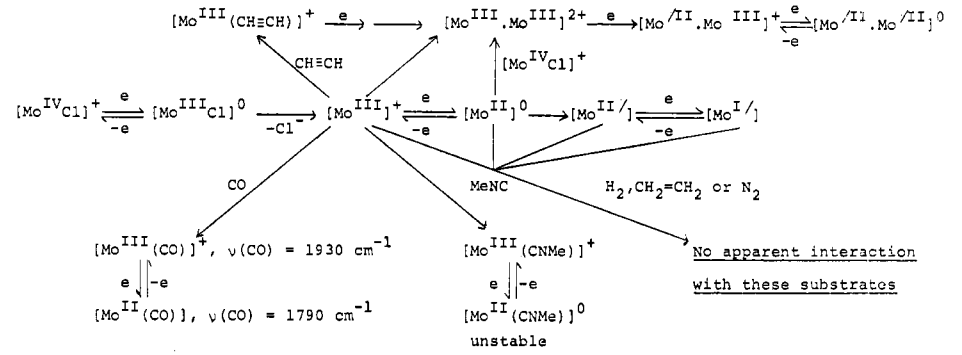

[a] Mo represents the core $[Mo(S_2CNR_2)_2(dppe)]$.

Table IX. Rate Constant Data[a]

$$[Mo^{III}Cl] \xrightarrow{K_1} [Mo^{III}]^+ + Cl^-$$

complex	solvent	K_1 (apparent), s^{-1}
$[MoCl(S_2CNEt_2)_2(dppe)][BF_4]$	MeCN	218
$[MoCl(S_2CNEt_2)(dppe)][BF_4]$	THF	19
$[MoCl(S_2CNEt_2)_2(PPh_2Me)_2][PF_6]$	MeCN	23
$[MoCl(S_2CNEt_2)_2(PPh_2Me)_2][PF_6]$	THF	2.6
$[Mo(CO)(S_2CNEt_2)_2(dppe)]$	THF	0.2[b]

[a] Estimated by double-potential-step technique in solvent containing 0.2 M $[NBu_4][BF_4]$. [b] Refers to loss of CO under 1 atm of CO.

is now discussed in detail in terms of the redox processes (1–5, Figure 2). The primary process (1, Figure 2) is a single-electron transfer, which is electrochemically reversible at fast scan rates (Figure 3). Controlled-potential electrolysis of $[MoCl]^+$ at potentials ${}^1E_p$ of −50 mV at a Pt electrode in THF or CH_3CN electrolytes consumes 1 faraday/mol of $[MoCl]^+$ and gives the *product* also obtained by chemical reduction, the dimeric $[\{Mo(S_2CNEt)_2(dppe)\}_2]$ complex, $[Mo^{III}Mo^{III}]^{2+}$. This species was identified by its distinctive cyclic voltammetric behavior (processes 3 and 4, Figure 2). The primary electron-transfer process (1, Figure 2) and the subsequent chemistry are therefore reasonably represented by eq 1. Whether

$$[Mo^{IV}Cl]^+ \underset{-e^-}{\overset{e^-}{\rightleftharpoons}} [Mo^{III}Cl]^0 \xrightarrow[K_1]{-Cl^-} [Mo^{III}]^+ \xrightarrow{\text{slow}} {}^1/_2[Mo^{III}Mo^{III}]^{2+} \quad (1)$$

or not $[Mo^{III}]^+$ is solvated by CH_3CN is not absolutely clear: the similarity of the redox potentials for $[MoCl]^+$ in either CH_3CN or THF suggests that it is not. We have determined the (apparent) rate constant for the first-order loss of halide ion, k_1, by the double-potential-step technique in both CH_3CN and THF.[16] From these data, listed in Table IX, it can be seen that the rate of loss of halide ion in CH_3CN is 1 order of magnitude faster than its rate of loss from $[MoCl]^0$ in THF, the solvent of lower dielectric constant. Similar solvent effects on reversibility have been observed in other systems in which a metal–halide bond ionizes following single-electron transfer.[17]

Cyclic voltammetry and controlled-potential electrolysis experiments show that the dimerization reaction, eq 1, which gives rise to product waves 3 and 4 (Figure 2) is a relatively slow process. The $[Mo^{III}]^+$ intermediate is therefore sufficiently long-lived to undergo independent redox chemistry as is shown by reduction processes 2 and 5 (Figure 2). The one-electron-transfer step (process 2, Figure 2) is quasi-reversible; its subsequent chemistry gives a product that reduces

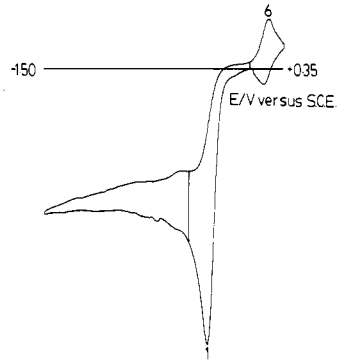

Figure 4. Cyclic voltammogram of $[MoCl(S_2CNEt_2)_2(dppe)][BF_4]$ (I) (under CO, 0.01 V s^{-1}, 2.5 mmol dm^{-3}, Pt, 0.2 M $[n\text{-}Bu_4N][BF_4]$–CH_3CN).

reversibly at ca. −1.2 V vs. SCE (process 5, Figure 2). In outline, these processes are consistent with eq 2; although we

$$[Mo^{IV}Cl]^+ \underset{-e^-}{\overset{(1)\ e^-}{\rightleftharpoons}} [Mo^{III}Cl]^0 \xrightarrow{-Cl^-} [Mo^{III}]^+ \underset{-e^-}{\overset{(2)\ e^-}{\rightleftharpoons}} [Mo^{II}]^0 \xrightarrow{(5)} [{}'Mo^{II}] \underset{-e^-}{\overset{e^-}{\rightleftharpoons}} [{}'Mo^{I}]^- \quad (2)$$

have not investigated them in detail, a structural rearrangement following the initial electron transfer seems likely, e.g. loss of weakly bound CH_3CN or isomerization.

Controlled-potential electrolysis at a Pt cathode in a CH_3CN electrolyte at potentials just negative of ${}^2E_p^{RED}$ (process 2, Figure 2) shows nonlinear charge passed vs. current decay characteristics. Initially, the reduction tends toward 2 faradays/mol of $[MoCl]^+$ but terminates close to 1 faradays/mol. The product of reduction is also the dimer $[Mo^{III}Mo^{III}]^{2+}$. Presumably the Mo^{II} species generated in the reduction step 2 of eq 2 attacks starting material, $[MoCl]^+$, or disproportionates to afford the dimer.

The redox chemistry of $[MoCl]^+$ is summarized in Scheme I, and redox potential data are listed in Table VI (supplementary material).

Under Carbon Monoxide. The cyclic voltammetry of $[MoCl(S_2CNR_2)_2(dppe)]^+$ under carbon monoxide in an acetonitrile electrolyte at a Pt electrode is illustrated for R = Et in Figure 4. The peak current for the primary process (1, Figure 4) is nearly double the height observed under argon, while all secondary redox features (processes 2–5, Figure 2) are essentially removed. In addition, a reversible one-electron oxidation process is observed for the reduction product at ${}^2E_{1/2}^{OX} = +0.16$ V, which we have identified as that of the $[Mo^{II}(CO)(S_2CNEt_2)_2(dppe)]^{0/+}$ couple (Figure 4). Con-

(16) Schwarz, W. M.; Shain, I. *J. Phys. Chem.* **1965**, *69*, 30.
(17) Bottomley, L. A.; Kadish, K. M. *Inorg. Chem.* **1981**, *20*, 1348.

trolled-potential electrolysis is an overall two-electron process in a CH_3CN electrolyte and not unexpectedly yields the Mo^{II} carbonyl. The mechanism of this reaction undoubtedly involves the binding of CO to the $[Mo^{III}]^+$ intermediate, followed by further rapid one-electron reduction at the negative potential of the primary process (1, Figure 4), eq 3. In previous work,

$$[Mo^{IV}Cl]^+ \xrightarrow{e^-} \xrightarrow{-Cl^-} [Mo^{III}]^+ \xrightarrow{CO} [Mo^{III}(CO)]^+ \underset{-e^-}{\overset{e^-}{\rightleftharpoons}} [Mo(CO)]^0 \quad (3)$$

we have shown that the $[Mo^{III}(CO)]$ intermediate is stable below 0 °C.[18] We have now estimated the apparent rate constant for its decomposition to be about 0.2 s^{-1} under 1 atm of CO at 20 °C by the double-potential-step method in an acetonitrile electrolyte (Table IX).

Under N_2. Cyclic voltammetry in an autoclave containing N_2 at 100 atm of pressure is indistinguishable from that observed for $[MoCl(S_2CNEt_2)_2(dppe)]^+$ in THF or CH_3CN electrolytes under argon. Evidently, N_2 does not interact with the electrogenerated Mo^{III}, Mo^{II}, or Mo^{I} intermediates.

In Acetylene-Saturated Solutions. Cyclic voltammetry of $[MoCl(S_2CNEt_2)(dppe)]^+$, in an acetonitrile electrolyte saturated with CH≡CH at 1 atm, mimics that observed under CO insofar as the secondary processes (2–5, Figure 2) are eliminated and the primary reduction current is increased toward that of a two-electron process. Controlled-potential electrolysis of $[MoCl]^+$ (R = Et) at a Pt electrode in a CH_3CN electrolyte saturated with acetylene at a potential ^1E_p of −100 mV tends toward a two-electron process in the early stage of electrolysis but terminates nearer 1 faraday/mol of $[MoCl]^+$. The product of electrolysis was identified as the *dimer*, formed in about 70% yield (eq 4). The fate of the (coordinated)

$$[Mo^{IV}Cl]^+ \xrightarrow{e^-} \xrightarrow{-Cl} [Mo^{III}]^+ \xrightarrow{CH\equiv CH} [Mo^{III}(CH\equiv CH)]^+ \xrightarrow{e^-} [Mo^{II}(CH\equiv CH)] \rightarrow \rightarrow \underset{\text{unstable}}{} [Mo^{III}Mo^{III}] \quad (4)$$

CH≡CH is unknown: it is not reduced to ethylene in significant amounts. Thus, controlled-potential electrolysis of $[MoCl]^+$ in 80% CH_3CN–MeOH containing 0.2 M $[NBu_4][BF_4]$ under 1 atm of CH≡CH gave only a 4% conversion of the acetylene to ethylene.

In the Presence of MeNC. Again, MeNC had an effect upon the cyclic voltammetry of $[MoCl]^+$ (R = Et) in a CH_3CN electrolyte, analogous to that observed for CO. A reversible reduction process was observed at −0.32 V for the product that we assign to the $[Mo(CH_3NC)(S_2CNEt_2)_2(dppe)]^{0/+}$ couple: the isocyanide complex is unstable on the time scale of controlled-potential electrolysis.

Electrochemical Reduction of Complexes $[MoCl(S_2CNEt_2)_2(P)_2]^+$ (P = PMe_2Ph, PEt_2Ph, or PPh_2Me). Table VIII litsts the primary reduction potential data for the $[MoCl]^+$ complexes studied. The monophosphine complexes are substantially harder to reduce than the diphosphine species. In addition, the stabilities of the one-electron-reduction products of the monophosphine series, $[Mo^{III}Cl]^0$ (Figure 5), are substantially more stable than the diphosphine species, which possess a different stereochemistry. Table IX shows rate constant data for the apparent first-order decomposition of $[MoCl(S_2CNEt_2)_2(PPh_2Me)_2]$ in THF and CH_3CN electrolytes. As with the diphosphine complex, the solvent effect is pronounced; however, in *either* solvent the rate of decay of

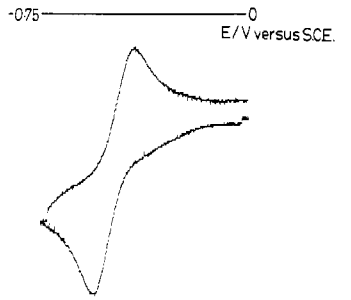

Figure 5. Cyclic voltammogram of $[MoCl(S_2CNEt_2)_2(PPh_2Me)_2][PF_6]$ (VII) (30 V s^{-1}, Pt, 2.3 mmol dm^{-3}, 0.2 M $[n\text{-}Bu_4N][BF_4]$–CH_3CN).

the diphosphine $[Mo^{III}Cl]$ species is 1 order of magnitude faster than is the decomposition of the monophosphine complex. We have not investigated the products of electrolysis of the monophosphine series although we have examined the effects of CO and CH≡CH on their cyclic voltammetry and have found that these gases, at 1 atm, have little effect in comparison with cyclic voltammograms recorded under argon in THF or MeCN electrolytes. This cannot altogether be due to the inherent stability of the $[MoCl]^0$ species: $[MoCl(S_2CNEt_2)_2(PPh_2Me)_2]^0$ has an estimated half-life of 30 ms or so in CH_3CN–0.2 M $[NBu_4][BF_4]$; therefore, *if* CO interacts rapidly with the $[Mo^{III}]^+$ product, we should have been able to detect this.

Conclusions

The complex $[Mo^{II}(CO)(S_2CNEt_2)_2(dppe)]$ has a comparatively low ν(CO), 1790 cm^{-1}, and on this ground alone we might expect a stable, or at least detectable, $[Mo^{II}(N_2)(S_2CNEt_2)_2(dppe)]$ species. That the CO species is readily synthesized via chemical or electrochemical reduction of the $[Mo^{IV}Cl]$ precursor, whereas the N_2 complex is not, probably lies with the inability of N_2 to bind the intermediate Mo^{III} oxidation level. The complex $[Mo^{III}(CO)(S_2CNEt_2)(dppe)]^+$ has a half-life on the order of a few seconds at 20 °C: we would expect the N_2 analogue to be substantially more labile. For example, *trans*-$[Mo(N_2)_2(dppe)_2]^+$ has a half-life of ca. 16 s at 20 °C whereas its dicarbonyl analogue is indefinitely stable under similar conditions.

The substrates CO, MeNC, and CH≡CH all bind to the Mo^{III} site in $[Mo(S_2CNEt_2)_2(dppe)]^+$ and promote further one-electron reduction of the molybdenum center to the Mo^{II} state at relatively low reduction potentials. Here we might note that the oxidation level at which the substrates CO, CH≡CH, and MeNC bind to the postulated Mo center(s) in nitrogenase, which is generally considered to be the N_2 binding and activating site, need not be as reduced as that to which N_2 binds. Furthermore, each of these substrates is capable of promoting the $Mo^{III} \rightarrow Mo^{II}$ reduction at relatively low potentials by virtue of their π^*-accepting capacity.

The reduction chemistry of $[MoCl(S_2CNR_2)_2(dppe)]^+$ (R = Me or Et) as we presently understand it is summarized in Scheme I.

Experimental Section

All reactions and manipulations were carried out in dry solvents under dinitrogen. $[MoO_2(S_2CNR_2)_2]$ and $[MoOCl_2(S_2CNR_2)_2]$ were prepared by established methods.[20,21] IR spectra were recorded on a Unicam SP2000 or SP1200 spectrophotometer as Nujol mulls. Conductivities were measured with a Portland Electronics conductance bridge with a standard cell in methyl cyanide as solvent. Room-temperature magnetic susceptibilities were measured in the solid state

(18) Crichton, B. A. L.; Dilworth, J. R.; Pickett, C. J.; Chatt, J. *J. Chem. Soc., Dalton Trans.* **1981**, 892.
(19) Leigh, G. J.; Pickett, C. J. *J. Chem. Soc., Dalton Trans.* **1977**, 1797.
(20) Jowitt, R. N.; Mitchell, P. C. H. *J. Chem. Soc. A* **1970**, 1702.
(21) Newton, W. E.; Bravard, D. C.; McDonald, J. W. *Inorg. Nucl. Chem. Lett.* **1975**, *11*, 553.

with an automatic recording balance calibrated with mercury cobalt thiocyanate. Microanalyses were made by Mr. and Mrs. A. Olney of the University of Sussex.

The Roman numerals correspond to those used in Table I.

Chlorobis(diethyldithiocarbamato)[bis(diphenylphosphino)-ethane]molybdenum(IV) Tetrafluoroborate (I). Bis(diphenylphosphino)ethane (dppe) (5.0 g, 0.0125 mol) was added to a suspension of oxodichlorobis(diethyldithiocarbamato)molybdenum(VI), $[MoOCl_2(S_2CNEt_2)_2]$ (2.4 g, 0.005 mol), in methanol (250 mL). The mixture was stirred for ca. 2 h, giving a brown-green solution and a small quantity of violet precipitate. The solution was then filtered, and tetra-*n*-butylammonium tetrafluoroborate, $[Bu_4N][BF_4]$ (1.7 g, 0.005 mol) was added to the filtrate. After evaporation to half the original volume, an olive green product precipitated, which crystallized as dark green needles from dichloromethane–diethyl ether; 3.1 g, 67%.

Complexes II–XI were prepared analogously from the appropriate starting complex and tertiary phosphine in yields of approximately 65%.

Dichlorobis(diethyldithiocarbamato)(dimethylphenylphosphine)-molybdenum(IV) (XII). Dimethylphenylphosphine (1.38 g, 0.010 mol) was added to a suspension of oxodichlorobis(diethyldithiocarbamato)molybdenum(IV) (2.4 g, 0.005 mol) in tetrahydrofuran. The resulting mixture was refluxed for 1 h. After the mixture cooled to room temperature, the green product precipitated from solution and was recrystallized as green needles from dichloromethane–propan-2-ol; 2.3 g, 75%.

Complexes XII–XV were prepared analogously in similar yields.

Tetrakis(dimethyldithiocarbamato)bis[[bis(diphenylphosphino)-ethane]molybdenum(III)] Tetrafluoroborate (XVI). Complex V (0.5 g) was suspended in dry methanol (25 mL) under argon and granulated tin (0.5 g) added. After being stirred for 1 h, the green-brown solution turned dark orange. The solution was filtered to remove excess tin and the solvent removed in vacuo. The residue was triturated with diethyl ether (20 mL) and the orange crude product filtered and recrystallized as red-orange chunky prisms from dichloromethane–diethyl ether (0.15 g, 30%).

Complexes XVIII–XIX were prepared by precipitation of the appropriate salt from the reaction solution with sodium tetraphenylborate or tetrabutylammonium hexafluorophosphate in 50–80% yield.

Carbonylbis(diethyldithiocarbamato)[bis(diphenylphosphino)-ethane]molybdenum(III). Granulated tin (0.5 g) was added to a stirred suspension of complex I (0.5 g) in dry methanol (25 mL) under carbon monoxide. After 1 h, the bright orange solution was evaporated to dryness in vacuo and the residue dissolved in dichloromethane (5 mL). The product was then crystallized as bright orange prisms by addition of methanol (3 mL); 0.2 g, 40%.

Crystal Preparation and Collection and Reduction of Diffraction Data. Olive green needles of $[MoCl(S_2CNEt_2)_2(dppe)][BF_4]$ and orange needles of $[MoCl(S_2CNEt_2)_2(PMe_2Ph)_2][PF_6]$ were formed by diffusion of diethyl ether into dichloromethane and mounted along the crystal axis. Preliminary cell dimensions were obtained from Weissenberg and precession photographs of the crystals taken with Cu Kα (λ = 1.5418 Å) radiation. Accurate cell dimensions were obtained by least-squares refinement of setting angles for 25 automatically centered, high-angle reflections. Intensity data were collected on a Nonius CAD4 computer-controlled diffractometer, using an $\omega/2\theta$ scan and Cu Kα radiation in a manner described in detail elsewhere;[22] fluctuations in the intensities of control reflections were no greater than those expected statistically. All data were corrected for Lorentz and polarization effects, but only intensity data for $[MoCl(S_2CNEt_2)_2(dppe)][BF_4]$ were corrected for absorption. The crystal data and cell parameters are given in Table III.

Solution and Refinement of the Structures. In both cases the position of the molybdenum atom was revealed by analysis of the initial Patterson map. The positional coordinates were used to produce a set of phased structure factors for a different Fourier synthesis, revealing the positions of the sulfur, phosphorus, and chlorine atoms in the coordination sphere of the molybdenum atom. These positional coordinates were refined by least-squares methods for four cycles, and Fourier synthesis of the phased structure factors now obtained resulted in the location of all the non-hydrogen atoms in the molecules under investigation. Anisotropic temperature factors were introduced for Mo, S, P, and Cl, and four cycles of refinement on the positional parameters and temperature factors led to convergence at values of 0.068 and 0.098 for the discrepancy factor $R = \sum||F_o| - |F_c||/\sum|F_o|$. Anisotropic temperature factors were not introduced for the carbon atoms in either structure.

Final positional and thermal parameters and observed and calculated structure factor amplitudes are available as supplementary material.

Electrochemistry. Cyclic voltammetry was carried out in oxygen-free electrolytes under an atmosphere of argon, dinitrogen, carbon monoxide, or acetylene by using a two-compartment, three-electron electrochemical cell, a Hi-Tek Instruments Ltd. DT2101 potentiostat, and a Chemical Electronics (Birtley) Ltd. Type 01 waveform generator. Voltammograms were recorded on a Philips PM8041 or Bryans 24000 X-Y recorder at ambient temperatures, 20 ± 2 °C. Cyclic voltammetry at 100 atm of dinitrogen was performed by using a mixture of nitrogen–argon gas over a conventional two-compartment, three-electron electrochemical cell in a specially adapted autoclave vessel and a Princeton Applied Research Ltd. Model 174A polarographic analyzer.

Controlled-potential electrolyses were performed in an H-type three-electrode, three-compartment cell with a working electrolyte volume of 20 mL. Platinum-gauze working and auxiliary electrodes of nominally 1 cm^2 were employed. Electrolyses were carried out on 30–80 μmol of complex under an argon, dinitrogen, or acetylene atmosphere, and the carge passed was measured with a Chemical Electronics integrator. In the case of electrolyses under acetylene in 80% MeCN–20% MeOH solvent, an aliquot (1 mL) of the gas space in the cell was removed after each electrolysis. The sample was examined by GC on a Poropak N column at ca. 60 °C. Under these conditions acetylene has a retention time of ca. 2.1 min and ethylene ca. 0.9 min. Yields of ethylene were 3–4%.

Double-potential-step kinetic measurements were carried out on equipment for cyclic voltammetry described previously. Values of the step time, τ, were within 1 order of magnitude of the half-life of the reaction. Decay curves were stored in a Datalab transient recorder, Model DL901, and plotted on a Bryans 24000 X-Y recorder. Measurements were made at 20 ± 0.1 °C.

Acknowledgment. We thank Dr. M. B. Hursthouse of Queen Mary College, London, for diffractometer time and assistance in data collection, Dr. P. Hitchcock and Professor Sir R. Mason for computer time, and J. E. Tolhurst and P. T. Bishop for technique assistance. J.A.Z. thanks the NIH for support (Grants GM 22566 and GM 27459).

Registry No. I, 87336-30-9; II, 87336-31-0; III, 87336-32-1; IV, 87336-33-2; V, 87336-35-4; VI, 87336-37-6; VII, 87336-39-8; VIII, 87350-55-8; IX, 87336-41-2; X, 87336-43-4; XI, 87336-45-6; XII, 87336-46-7; XIII, 87336-47-8; XIV, 87336-48-9; XV, 87336-49-0; XVI, 87336-51-4; XVII, 87336-52-5; XVIII, 87336-53-6; XIX, 87336-55-8; $[Mo(CO)(S_2CNEt_2)_2(dppe)]$, 87392-58-3; $[MoOCl_2(S_2CNEt_2)_2]$, 57146-54-0; $[MoOCl_2(S_2CNMe_2)_2]$, 59491-19-9; $[MoOBr_2(S_2CNEt_2)_2]$, 53548-92-8; CO, 630-08-0; CH≡CH, 74-86-2; MeNC, 593-75-9.

Supplementary Material Available: Properties and analyses of complexes I–XV (Table I), final atomic positional and thermal parameters (Tables IVa and IVb), expanded listings of bond distances and angles (Table V continued), nonbonding interactions defining polyhedral edges (Tables VIa and VIb), and analyses and NMR data for complexes XVI–XIX (Table VII), and listings of observed and calculated structure factors (44 pages). Ordering information is given on any current masthead page.

(22) Bruce, A.; Corbin, J. L.; Dahlstrom, P. L.; Hyde, J. R.; Minelli, M.; Minelli, M.; Stiefel, E. I.; Spence, J. T.; Zubieta, J. *Inorg. Chem.* **1982**, *21*, 917.